

# AMUSE-VIRGO I. SUPER-MASSIVE BLACK HOLES IN LOW-MASS SPHEROIDS

ELENA GALLO<sup>1,2</sup>, TOMMASO TREU<sup>1,3</sup>, JEREMY JACOB<sup>1</sup>, JONG-HAK WOO<sup>1</sup>, PHILIP J. MARSHALL<sup>1,4</sup>, ROBERT ANTONUCCI<sup>1</sup>

*Draft version August 31, 2021*

## ABSTRACT

We present the first results from the AGN Multiwavelength Survey of Early-type galaxies in the Virgo cluster (AMUSE-Virgo). This large program targets 100 early-type galaxies with the Advanced CCD Imaging Spectrometer on board the *Chandra X-ray Observatory* and the Multi-band Imaging Photometer on board the *Spitzer Space Telescope*, with the aim of providing an unbiased census of low-level super-massive black hole activity in the local universe. Here we report on the *Chandra* observations of the first 16 targets, and combine them with results from archival data of another, typically more massive, 16 targets. Point-like X-ray emission from a position coincident with the optical nucleus is detected in 50 per cent of the galaxies (down to our completeness limit of  $\sim 4 \times 10^{38}$  erg s<sup>-1</sup>). Two of the X-ray nuclei are hosted by galaxies (VCC1178=N4464 and VCC1297=N4486B) with absolute B magnitudes fainter than  $-18$ , where nuclear star clusters are known to become increasingly common. After carefully accounting for possible contamination from low mass X-ray binaries, we argue that the detected nuclear X-ray sources are most likely powered by low-level accretion on to a super-massive black hole, with a  $\lesssim 11$  per cent chance contamination in VCC1178, where a star cluster is barely resolvable in archival *Hubble Space Telescope* images. Based on black hole mass estimates from the global properties of the host galaxies, all the detected nuclei are highly sub-Eddington, with luminosities in the range  $-8.4 < \log(L_{0.3-10 \text{ keV}}/L_{\text{Edd}}) < -5.9$ . The incidence of nuclear X-ray activity increases with the stellar mass  $M_*$  of the host galaxy: only between 3–44 per cent of the galaxies with  $M_* < 10^{10} M_\odot$  harbor an X-ray active super-massive black hole. The fraction rises to between 49–87 per cent in galaxies with stellar mass above  $10^{10} M_\odot$  (at the 95 per cent confidence level).

*Subject headings:* black hole physics – galaxies: nuclei – galaxies: clusters: individual (Virgo)

## 1. INTRODUCTION

One of the main recent developments in the study of galaxy formation and evolution has been the realization of the key role played by nuclear activity due to accretion onto super-massive black holes (SMBHs). Low-level accretion-powered activity has been suggested to be relevant for a variety of phenomena, including regulating star formation at galaxy scales via energy feedback to solve the ‘downsizing’ problem and providing extra energy to solve the ‘cooling flow’ problem (Cowie et al. 1996; Dalla Vecchia et al. 2004; Springel et al. 2004; Treu et al. 2005a,b; Bundy et al. 2005, 2007; Juneau et al. 2005; De Lucia et al. 2006; Abraham et al. 2007; Sijacki et al. 2007; McNamara & Nulsen 2007). The most compelling pieces of evidence supporting a strong connection between galaxy formation and nuclear activity are the tight empirical scaling relations connecting the mass of the central SMBH with global properties of the host galaxy, such as bulge luminosity and mass (Kormendy & Richstone 1995; McLure & Dunlop 2002; Marconi & Hunt 2003; Häring & Rix 2004), galaxy-light concentration (Graham et al. 2001; Erwin 2004), and stellar velocity dispersion (Gebhardt et al. 2000; Ferrarese & Merritt 2000). An issue of fundamental importance in understanding the galaxy-black hole connection is the ‘duty cycle’ of nuclear activity, and its dependence upon, e.g. black hole mass. If SMBHs are indeed ubiquitous in

galactic bulges, little is known about the frequency and intensity of nuclear activity, the more so at the low-mass end (see Greene & Ho 2007a). Even though a minimum level of accretion should be present, fueled by mass loss during stellar evolution (e.g. Ciotti et al. 1991; Ciotti & Ostriker 2007), the inferred accretion-powered luminosities are often lower than what expected from standard Bondi-Hoyle accretion (as found e.g. for the Galactic Center SMBH Sgr A\*; Baganoff et al. 2003).

From an empirical point of view, optical studies are mostly limited to samples of known active nuclei (e.g. Woo & Urry 2002; Heckman et al. 2004; Kollmeier et al. 2006; Greene & Ho 2007b) with limited coverage of the black hole mass-Eddington luminosity ( $M_{\text{BH}}\text{--}L_{\text{Edd}}$ ) plane. Prior to the launch of the *Chandra X-ray Observatory*, searches for low-level accretion powered X-ray emission from apparently inactive galaxies were effectively limited to X-ray luminosities  $\gtrsim 10^{40}$  erg s<sup>-1</sup> (e.g. Fabbiano & Juda 1997; Allen, Di Matteo & Fabian 2000; Sulkanen & Bregman 2001). The greatly improved *Chandra* sensitivity, together with its fine spatial resolution, has made it possible to investigate nuclear emission associated with SMBH activity down to 3 orders of magnitude deeper, effectively bridging the gap between active galactic nuclei (AGN) and inactive galaxies. Perhaps surprisingly, only very low levels of nuclear X-ray luminosity ( $L_X/L_{\text{Edd}} < 10^{-6}$ , 2–10 keV) have been observed in nearby *massive* ellipticals (Di Matteo et al. 2000; Ho et al. 2001; Loewenstein et al. 2001; Pellegrini 2005; Soria et al. 2006a,b; Santra et al. 2007), despite their containing vast fuel reservoirs in the form of hot X-ray emitting interstellar gas. While these results rule out radiatively efficient solutions for the accretion flow, the detected X-ray

<sup>1</sup> Physics Department, University of California Santa Barbara, CA 93106-9530

<sup>2</sup> Chandra Fellow

<sup>3</sup> Sloan Fellow, Packard Fellow

<sup>4</sup> Tabasgo Fellow

luminosities can vary by orders of magnitude when plotted against the Bondi accretion rate (Pellegrini 2005), with a large fraction of systems being even fainter than predicted by advection-dominated accretion flow models (Narayan & Yi 1994).

These observations are closely related to the role of SMBH feedback in inhibiting star formation at a galaxy scale level. Semi-analytical models applied to state of the art cold-dark-matter simulations have recently highlighted the importance of highly sub-Eddington SMBH activity. In the formulation by Croton et al. (2006), a low level of prolonged activity (the so-called ‘radio mode’) is essential to prevent the reservoir of gas surrounding the most massive galaxies from cooling and producing young stars, and thus reproduce their red colors. In this scenario, low-level SMBH feedback halts the gas supply to the disk from the surrounding hot halo, truncating star formation and allowing the existing stellar population to redden.

So far however, these studies have been sparse and necessarily focused on the small number of galaxies at the high-mass end of the local population. At the same time, while the paucity of AGN in the local universe is a known phenomenon, recent studies point towards an actual decline in the spatial density of local active black holes with mass below  $10^{6.5-7} M_{\odot}$  (Greene & Ho 2007b), possibly due to low black hole occupation fraction and/or low bulge fraction in dwarf galaxies. In turn, this can place constraints on the very mechanism by which SMBHs formed in the early universe, since different models for the formation of black hole seeds predict different black hole occupation fractions at redshift zero. This effect becomes more prominent down the mass function. In particular, models where the black hole seeds are formed in the nuclei of gravitationally unstable pre-galactic discs that form through the collapse of haloes at redshift  $\sim 10$  (e.g., Madau & Rees 2001, Begelman et al. 2006, Lodato & Natarajan 2006) predict the existence of a population of faint low-mass galaxies with no black hole at their center (Volonteri et al. 2007a,b).

As a matter of fact, ‘light’ SMBHs, presumably harbored by faint dwarf galaxies, remain elusive: the strong limits placed by dynamical studies on the masses of the nuclear objects in M33 (Gebhardt et al. 2001; Merritt et al. 2001) and NGC205 (Valluri et al. 2005) suggest that neither galaxy hosts a SMBH of the mass expected from extrapolation of the known scaling relations in massive bright galaxies. Ferrarese et al. (2006a) suggest that, while SMBHs are common in bright (absolute B magnitude  $M_B < -20$ ) massive galaxies, they would be progressively replaced by compact stellar nuclei moving down the mass function, and may disappear entirely at the faint end. On the other hand, compelling evidence exists for a  $3.7 \times 10^6 M_{\odot}$  black hole at the center of our own Milky Way (Ghez et al. 2005), providing us with the best example of highly radiatively inefficient black hole accretion (the measured X-ray luminosity between 2–10 keV can be as low as  $10^{33.3} \text{ erg s}^{-1}$ ; Baganoff et al. 2003). Although no direct dynamical black hole mass determination exists below  $10^6 M_{\odot}$ , indirect evidence points towards the existence of such objects in active galaxies (Filippenko & Ho 2003; Peterson et al. 2005; Barth et al. 2004; Greene & Ho 2004, 2007a), globular clusters (Gebhardt et al. 2002, Gerssen et al. 2002) as well as

(some) ultra-luminous X-ray sources (Miller 2005).

In this paper we present the first results from an extensive multi-wavelength survey of 100 spheroids –elliptical, lenticular and dwarf spheroidal galaxies– in the Virgo cluster, conducted with the *Chandra X-ray Observatory* and the *Spitzer Space Telescope*: AMUSE-Virgo (AGN Multiwavelength Survey of Early-types in Virgo<sup>5</sup>). As described in § 2 the survey is designed to provide the first unbiased census of low levels of nuclear activity in the local universe as a function of host galaxy mass for early-type galaxies. § 3 describes our analysis of the new and archival *Chandra* data obtained so far (32/100 galaxies), as well as of archival *Hubble Space Telescope* (HST) images used to connect the X-ray detections with their optical counterparts and with the host galaxy properties. In § 4 we use the known correlations with host galaxy properties (stellar velocity dispersion  $\sigma$  and spheroid luminosity  $L_B$ ) to estimate masses for the central black holes. § 5 presents our main results, which are summarized in § 6.

## 2. AMUSE-VIRGO: PROGRAM DESCRIPTION

This *Chandra* Large Program (ID 08900784, Cycle 8, 454 ks; PI Treu) targets the 100 early-type galaxies of the ACS<sup>6</sup> Virgo Cluster Survey (ACSVCS; Côté et al. 2004), with the aim of providing an unbiased census of SMBH luminosity in the local universe. Mid-infrared observations with the Multi-band Imaging Photometer on board *Spitzer* (MIPS; total exposure 9.5 hrs) complete the X-ray survey, allowing us to probe obscured accretion-powered emission through 24  $\mu\text{m}$  observations.

The *Chandra* survey has been designed to be sensitive (at  $3\text{-}\sigma$ ) to a  $3 M_{\odot}$  object accreting at the Eddington limit. As described in detail in § 5, this is the optimal depth for an extensive survey: the threshold is deep enough to be interesting, yet bright enough to ensure negligible contamination by stellar mass black holes (or background sources) within the *Chandra* Point Spread Function (PSF). The desired sensitivity is accomplished by means of snapshot (5.4 ksec) observations of 84 targets. The new data are combined with deeper archival *Chandra* observations of the remaining (on average more massive) 16 targets.

Based on the comparison with the spectral energy distribution (SED) of LINERs (Low Ionization Nuclear Emitting Regions; see e.g. Maoz et al. 1998) and unobscured AGN (both radio loud and radio quiet), the mid-IR band flux is expected to exceed the *Chandra* flux by at least a factor 3. Hence, the *Spitzer* survey – which will acquire new data for 57 objects, to be combined with archival data for the remaining 43 – has been designed to probe down to  $\simeq 3 \times 10^{-14} \text{ erg sec cm}^{-2}$  (three times higher than the *Chandra* threshold).

Based on empirical scaling relations between the black hole mass and the host properties, the ACSVCS sample covers over 5 orders of magnitude in black hole mass as estimated from the mass-velocity dispersion relation (see § 3 for a critical assessment), large enough that it can be divided in SMBH mass bins to test whether the nuclear activity duty cycle is mass dependent; given our

<sup>5</sup> <http://tartu.physics.ucsb.edu/~amuse>

<sup>6</sup> Advanced Camera for Surveys, on board the *Hubble Space Telescope*.

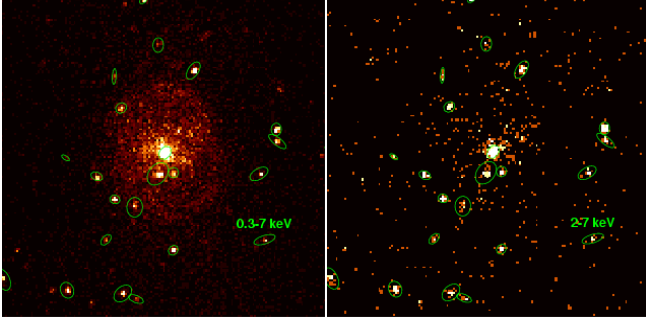


FIG. 1.— ACIS-S image of VCC1632 (=M89; 24.8 ksec of exposure). *Left*: 0.3–7 keV image. *Right*: 2–7 keV image, with negligible diffuse emission from the hot gas.

sensitivity, we will probe X-ray Eddington ratios in the range  $10^{-9} - 10^{-5}$ .

### 3. DATA ANALYSIS

In this section we report on the analysis of *Chandra* data for the 16 targets observed in Cycle 8 at the time of submission of this paper (§ 3.1), and on the analysis of the nuclear X-ray emission of the 16 galaxies of the survey that have archival *Chandra* data (§ 3.2). § 3.3 describes the analysis of archival HST data used to compare the location of X-ray detections to the optical center of the host galaxies (and nuclei when present), and to estimate their stellar mass. The target list and observation log are given in Table 1.

#### 3.1. *Chandra* Cycle 8 data

We observed each galaxy with the Advanced CCD Imaging Spectrometer (ACIS) detector on board *Chandra* for 5.4 ksec of nominal exposure time in Faint-mode. The target was placed at the aim point of the back-side illuminated S3 chip. We analyzed the data using the *Chandra* Interactive Analysis Observation (CIAO) software version 3.4.1.1 and the calibration database version 3.3.0.1. Standard level 2 event lists, processed for cosmic ray rejection and good time filtering, were employed. As *Chandra* is known to encounter periods of high background which especially affect the S1 and S3 chips, we first checked for background flares and removed time intervals with background rate  $\gtrsim 3\sigma$  above the mean level.

Further analysis was restricted to energies between 0.3–7.0 keV in order to avoid calibration uncertainties at low energies and to limit background contaminations at high energies. We applied a wavelet detection algorithm over each activated chip, using CIAO *wavdetect* with sensitivity threshold corresponding to a  $10^{-6}$  chance of detecting one spurious source per PSF element if the local background is uniformly distributed. We used the default wavelet parameters, with scales increasing by a factor of  $\sqrt{2}$ : between 1–4 pixels on a full resolution circular region of 512 pixel radius centered on the nominal position of the target (restricting the circle to the sole S3 chip), and between 1–8 pixels for a  $1''$  resolution image of each activated chip. The complete *Chandra* source catalog will be presented elsewhere; here we shall focus on the X-ray properties of the nuclei. Given the relatively short exposures ( $\sim 5.4$  ksec), we detect between 3 (VCC33) and 15 (VCC751) X-ray sources within a 512 pixel ( $\sim 252''$ ) aperture. A small fraction of them, often none, are enclosed within the HST ACS field of view

( $200 \times 200$  arcsec<sup>2</sup>); this prevents us from directly registering the *Chandra* data to HST. Thus, we first improved the *Chandra* astrometry by cross-matching the detected (non-nuclear) X-ray sources with the Sloan Digital Sky Survey (SDSS) catalog (Data Release 5, DR5), and applied the resulting bore-sight corrections following the method described by Zhao et al. (2005).

Individual source locations are subject to statistical uncertainties affecting the centroiding algorithm and to the dispersion of photons due to the PSF. For ACIS-S, Garmire et al. (2000) estimate 90 per cent confidences of  $\pm 0''.5$  for sources with  $\sim 10$  counts,  $\pm 0''.2$  for 20–50 count sources, and negligible for  $> 100$  count sources. In addition, the statistical uncertainties depend on the off-axis angle from the aim point: we calculated the 95 per cent confidence error radii,  $r_X$ , as a function of net counts and off-axis angle according to the empirical formula based on the results of Hong et al. (2005). The statistical uncertainties affecting the centroid errors in the positions of the X-ray sources, combined with the  $\lesssim 0''.1$  positional error of SDSS, results in a final astrometric frame that is accurate to between  $0''.2$  (fields with  $\gtrsim 20$  counts sources) and  $0''.5$  (fields with faint sources).

After registering the *Chandra* images to SDSS, we ran again *wavdetect* to refine the positions, and searched for point-like X-ray emission centered at the galaxy optical center, derived from archival HST ACS images registered to the SDSS world coordinate system as described in the next subsection. We searched for X-ray counterparts to the ACS nuclei within an error circle which is the quadratic sum of the positional uncertainty for the X-ray source, the uncertainty in the optical astrometry, and the uncertainty in the X-ray bore-sight correction, multiplied by the chosen confidence level scale factor ( $3\sigma$ ):

$$R_{\text{err}} = \sqrt{r_X^2 + r_{\text{opt}}^2 + r_{\text{bore}}^2} \quad (1)$$

The coordinates of the detected X-ray nuclei, with their statistical uncertainty, are listed in Table 1. More details about the optical astrometry are provided in § 3.3.

For the X-ray aperture photometry, we adopted a circular region with a  $2''$  radius centered on X-ray centroid position. For all the observations considered here, the aim-points were specified in order to have optimal nuclear positions with respect to CHIP geometry and telescope focus; thus,  $2''$  correspond to 95 per cent of the encircled energy radius at 1.5 keV for ACIS. We inspected the morphology of the detected nuclei by constructing the *Chandra* PSF at 1.5 keV and normalized it to the actual number of detected counts; all the detected X-ray nuclei in the Cycle 8 observations are consistent with being point-like.

We adopted an annulus with inner radius  $20''$  and outer radius  $30''$  for background subtraction (off-nuclear X-ray sources, if present, were masked out). We estimated the corresponding fluxes using *webPimms*<sup>7</sup>, and assuming an absorbed power-law model with photon index  $\Gamma = 2$  and

<sup>7</sup> <http://heasarc.gsfc.nasa.gov/Tools/w3pimms.html>

TABLE 1  
AMUSE-VIRGO I.: OBSERVATION LOG AND X-RAY NUCLEI

ID	VCC	Other	OID	Date	Exp.	X-ray Counts	$\alpha$ (J2000)	$\delta$ (J2000)	Opt Nucl. $\alpha$ (J2000)	$\delta$ (J2000)
(1)	(2)	(3)	(4)	(5)	(6)	(7)	(8)	(9)	(10)	(11)
1	1226	N4472	321 <sup>a</sup>	00-06-12	33.64	..	..	..	12:29:46.764	+08:00:01.75
2	1316	N4486	352, 2707, 3717	00-07-29, 02-07-06, 02-07-05	119.22	82011 <sup>b</sup> (961)	12:30:49.409 (0.01)	+12:23:28.20 (0.01)	12:30:49.425	+12:23:28.08
3	1978	N4649	785 <sup>a</sup>	00-04-20	34.31	151.3 <sup>b</sup> (61.2)	12:43:39.977 (0.02)	+11:33:10.05 (0.02)	12:43:39.989	+11:33:09.55
4	881	N4406	318	00-04-07	14.63	..	..	..	12:26:11.759	+12:56:46.44
5	798	N4382	2016	01-05-29	39.75	..	..	..	12:25:24.071	+18:11:27.92
6	763	N4374	6131 <sup>a</sup>	05-11-07	38.75	705 <sup>b</sup> (63)	12:25:03.746 (0.04)	+12:53:13.30 (0.04)	12:25:03.743	+12:53:13.01
7	731	N4365	5921 <sup>a</sup>	05-04-28	39.51	84.8 <sup>b</sup> (27)	12:24:28.289 (0.06)	+07:19:04.03 (0.06)	12:24:28.271	+07:19:03.99
8	1535	N4526	3925 <sup>a</sup>	03-11-14	38.39	..	..	..	12:34:03.029	+07:41:57.62
9	1903	N4621	2068	01-08-01	24.84	167.4 <sup>b</sup> (30.5)	12:42:02.242 (0.06)	+11:38:49.17 (0.06)	12:42:02.262	+11:38:48.87
10	1632	N4552	2072 <sup>a</sup>	01-04-22	54.13	933 <sup>b</sup> (82)	12:35:39.811 (0.02)	+12:33:22.81 (0.02)	12:35:39.811	+12:33:22.74
11	1231	N4473	4688 <sup>a</sup>	05-02-26	29.58	58.7 <sup>b</sup> (13.6)	12:29:48.864 (0.12)	+13:25:45.19 (0.17)	12:29:48.870	+13:25:45.95
12	2095	N4762	3998 <sup>a</sup>	03-05-17	5.31	11.8 (3.5)	12:52:55.979 (0.10)	+11:13:51.63 (0.09)	12:52:56.045	+11:13:51.87
13	1154	N4459	2927	02-06-02	9.83	48.3 (7)	12:29:00.027 (0.13)	+13:58:42.56 (0.12)	12:29:00.030	+13:58:42.90
15	2092	N4754	8038	07-02-19	4.97	8.7 (2.9)	12:52:17.496 (0.14)	+11:18:49.99 (0.19)	12:52:17.50	+11:18:49.97
18	1692	N4570	8041	07-04-28	5.09	5.7 (2.4)	12:36:53.378 (0.14)	+07:14:47.98 (0.22)	12:36:53.398	+07:14:47.57
21	685	N4350	4015	04-02-28	4.7	27.8 (5.3)	12:23:57.869 (0.15)	+16:41:36.42 (0.17)	12:23:57.848	+16:41:36.21
22	1664	N4564	4008 <sup>a</sup>	03-11-21	17.86	74.6 <sup>b</sup> (9)	12:36:26.990 (0.11)	+11:26:21.70 (0.10)	12:36:26.995	+11:26:21.04
27	1720	N4578	8048	07-04-28	5.09	..	..	..	12:37:30.561	+09:33:18.19
30	1883	N4612	8051	07-04-16	5.09	4.8 (2.2)	12:41:32.743 (0.18)	+07:18:52.93 (0.26)	12:41:32.751	+07:18:53.48
42	1913	N4623	8062	07-05-11	5.28	..	..	..	12:42:10.688	+11:38:48.87
46	1178	N4464	8127	07-04-29	5.09	10.8 (3.3)	12:29:21.297 (0.21)	+08:09:23.80 (0.17)	12:29:21.289	+08:09:23.81
51	2048	I3773	8070	07-04-28	5.28	..	..	..	12:47:15.293	+10:12:12.82
53	9	I3019	8072	07-04-13	5.28	..	..	..	12:09:22.340	+13:59:33.10
56	1049	U7580	8075	07-04-28	5.51	..	..	..	12:27:54.836	+08:05:25.40
61	1297	N4486B	4007 <sup>a</sup>	03-11-21	36.18	42.2 <sup>b</sup> (8.2)	12:30:31.966 (0.08)	+12:29:24.64 (0.07)	12:30:31.969	+12:29:24.57
67	1833	—	8084	07-03-17	5.25	..	..	..	12:40:19.670	+15:56:06.76
70	33	I3032	8086	07-02-01	5.16	..	..	..	12:11:07.755	+14:16:29.20
76	1895	U7854	8092	07-04-28	5.09	..	..	..	12:41:51.964	+09:24:10.33
80	1857	I3647	8130	07-04-29	5.09	..	..	..	12:40:53.095	+10:28:33.46
86	2050	I3779	8101	07-05-07	5.09	..	..	..	12:47:20.638	+12:09:59.12
88	751	I3292	8103	07-04-13	5.09	..	..	..	12:24:48.363	+18:11:42.44
93	1199	—	8107	07-04-28	5.09	..	..	..	12:29:34.998	+08:03:28.81

NOTE. — Col.: (1) ACSVCS target number (2) VCC source name; (3) Other name (4) *Chandra* Observation Identity; (5) Observation starting date; (6) Net exposure (after flares' removal) (7) Nuclear X-ray source: net counts extracted –or extrapolated to– between 0.3–7 keV; (8) X-ray Nucleus R.A. (J2000), with the positional uncertainty on the centroid position given in parenthesis, in arcsec (9) X-ray Nucleus Dec (J2000) with the positional uncertainty on the centroid position given in parenthesis, in arcsec; (10) Optical nucleus R.A. (J2000); (11) Optical nucleus Dec (J2000).  
a): Very Faint mode; b) In order to avoid contamination from the diffuse gas emission, the nuclear counts were extracted between  $E_t$ -7 keV (see § 3.2), where typically  $E_t \gtrsim 2$  keV, and then extrapolated to between 0.3–7 keV within *webPimms* adopting an absorbed power law model with Galactic absorption and photon index  $\Gamma = 2$ .

hydrogen equivalent column  $N_H = 2.5 \times 10^{20} \text{ cm}^{-2}$ , i.e. the nominal Galactic value determined from the HI studies of Dickey & Lockman (1990). Since none of galaxies under exam shows evidence for prominent dusty lanes in the Hubble images (Ferrarese et al. 2006b), it is reasonable to assume that the Galactic value provides a correct estimate for the actual absorbing column. Under this assumptions,  $10^{-3} \text{ count s}^{-1}$  in the 0.3-7 keV energy band correspond to an intrinsic flux of  $7.19 \times 10^{-15} \text{ erg cm}^{-2} \text{ s}^{-1}$  between 0.3-10 keV (ACIS-S).

In case of no significant detection we applied Poisson statistics to derive upper limits on the nuclear luminosity at the 95 per cent confidence level (Gehrels 1986), listed in Table 2. To obtain a more stringent limit on the average flux, we stacked the images of the non-detections centered on the optical centers, resulting in 62.3 ks of effective total exposure. We extracted the counts from a  $2''$  radius circular aperture, and background from an annulus with inner and outer radii  $R_{\text{in}} = 2''$  and  $R_{\text{out}} = 9''$ , centered on the stacked nucleus position (see Figure 2). We found 5 counts within the  $2''$  radius aperture, while

3.1 are expected from the background. The Poisson probability of obtaining 5 counts or more when 3.1 are expected is 0.2, indicating no significant detection. This corresponds to an exposure weighted, *average* count rate  $< 1.6 \times 10^{-4} \text{ count s}^{-1}$  for the undetected sources (95 per cent confidence level), or  $\langle L_X \rangle < 3.8 \times 10^{37} \text{ erg s}^{-1}$  (0.3–10 keV) at the average distance of 16.5 Mpc (Mei et al. 2007).

### 3.2. *Chandra* archival data

We followed the same procedure as outlined above for the 16 galaxies which have *Chandra* archival data (marked by an *a* superscript in Table 2). For these targets, event 1 lists were first filtered (and cleaned, in the case of Vary Faint telemetry) following the standard CIAO threads. As the archival sample is mainly made of massive, X-ray bright galaxies, we had to model/account for the diffuse gas contribution in order to constrain any possible accretion-powered, nuclear X-ray emission. This was achieved by first determining for each galaxy the energy  $E_t$  above which hot gas contribution is negligible.

TABLE 2  
AMUSE-VIRGO I.: NUCLEAR PROPERTIES

ID	VCC	Other	$d$	B	$\sigma$	$\log M_{\text{BH},\text{B}}$	$\log M_{\text{BH},\sigma}$	$\log L_{\text{X,nucl}}$	$\log M_{\star}$
(1)	(2)	(3)	(Mpc) (4)	(mag) (5)	(km/s <sup>-1</sup> ) (6)	(M <sub>⊙</sub> ) (7)	(M <sub>⊙</sub> ) (8)	(erg s <sup>-1</sup> ) (9)	(10)
1	1226 <sup>a</sup>	M49, N4472	17.14	8.63	308±9	9.4	9.1	<38.49 (14,15)	12.0
2	1316 <sup>a</sup>	M87, N4486	17.22	9.05	355±8	9.2	9.4	41.20 (16,17)	11.8
3	1978 <sup>a</sup>	M60, N4649	17.30	9.33	347±9	9.1	9.4	39.05 (18)	11.7
4	881 <sup>a</sup>	M86, N4406	16.83	8.77	245±11	9.3	8.6	<38.64	11.9
5	798 <sup>a</sup>	M85, N4382	17.86	9.30	205±8	9.2	8.3	<38.43 (19)	11.6
6	763 <sup>a</sup>	M84, N4374	18.45	9.35	297±7	9.2	9.0	39.73 (20)	11.7
7	731 <sup>a</sup>	N4365	23.33	9.98	261±7	9.1	8.8	39.0 (19)	11.7
8	1535 <sup>a</sup>	N4526	16.50	10.52 <sup>b</sup>	316±7	8.6	9.2	<38.21	11.0
9	1903 <sup>a</sup>	M59, N4621	14.93	10.02	233±7	8.7	8.5	39.11	11.3
10	1632 <sup>a</sup>	M89, N4552	15.85	10.13	257±18	8.7	8.7	39.58 (21)	11.3
11	1231 <sup>a</sup>	N4473	15.27	11.19	189±10	8.2	8.1	38.60 <sup>c</sup>	10.8
12	2095 <sup>a</sup>	N4762	16.50	11.97	147±10 (12)	8.0	7.6	38.71	10.6
13	1154 <sup>a</sup>	N4459	16.07	11.07	170±12	8.3	7.9	39.03 (22)	10.9
15	2092	N4754	16.14	11.36	200±10 (12)	8.2	8.2	38.59	10.9
18	1692	N4570	17.06	11.91	180±18	8.0	8.0	38.45	10.6
21	685 <sup>a</sup>	N4350	16.50	11.83	198±9	8.0	8.2	39.14 (23)	10.6
22	1664 <sup>a</sup>	N4564	15.85	11.85	157±9	8.0	7.7	39.95 (24)	10.6
27	1720	N4578	16.29	12.01	153±15	8.0	7.6	<38.54	10.4
30	1883	N4612	16.59	12.01	104±11 (12)	8.0	6.8	38.35	10.4
42	1913	N4623	17.38	13.16	89±10 (12)	7.5	6.5	<38.46	10.1
46	1178	N4464	15.85	13.32	121±25 (13)	7.4	7.1	38.67	9.9
51	2048	I3773	16.50	14.04	79±5	7.1	6.3	<38.12	9.5
53	9	I3019	17.14	14.00	..	7.2	..	<38.15	9.7
56	1049	U7580	15.99	14.93	..	6.7	..	<38.08	9.0
61	1297 <sup>a</sup>	N4486B	16.29	14.14	166±8	7.1	7.8	38.42 (24)	9.7
67	1833	—	16.22	14.66	..	6.8	..	<38.11	9.3
70	33	I3032	15.07	15.22	..	6.5	..	<38.25	8.9
76	1895	U7854	15.85	15.15	..	6.6	..	<38.10	9.0
80	1857	I3647	16.50	15.06	..	6.7	..	<38.14	9.4
86	2050	I3779	15.78	15.37	..	6.5	..	<38.10	9.0
88	751	I3292	15.78	14.86	..	6.7	..	<38.29	9.4
93	1199	—	16.50	16.00	..	6.3	..	<38.14	9.0

NOTE. — Col.: (1) ACSVCS target number (2) VCC source name; (3) Alternate name, from NCG or catalogs; (4) Distance (from surface brightness fluctuations method; Mei et al. 2007). The average distance to the Virgo cluster – of 16.5 Mpc – is employed in case of no available distance modulus; (5) Extinction-corrected B magnitude, estimated as described in § 3.3; E(B-V) values are from Ferrarese et al. (2006b); (6) Stellar velocity dispersion, from ENEARc (Bernardi et al. 2002), unless otherwise indicated; (7) B-based black hole mass, adopting the scaling by FF05 (8)  $\sigma$ -based black hole mass, adopting the scaling by FF05; (9) Nuclear luminosity between 0.3-10 keV, corrected for absorption; literature references are given in brackets; (10) Stellar mass of the host galaxy, in M<sub>⊙</sub>, derived from  $g_0$  and  $z_0$  band AB model magnitudes following Bell et al. (2003), as described in § 3.3.

References 11) Gavazzi et al. 1999 (Ga99); 13) Davies et al. 1987 (D87); 14) Biller et al. 2004; 15) Soldatenkov et al. 2003; 16) Di Matteo et al. 2003; 17) Wilson & Yang 2002; 18) Randall et al. 2004 report on a point-like X-ray source at 1''.6 from the nucleus. After cross-matching the *Chandra* astrometry to SDSS, the position of the nuclear X-ray source is found to be consistent with the galaxy nucleus; 19) Sivakoff et al. 2003; 20) Finoguenov & Jones 2001; 21) Xu et al. 2005; 22) Satyapal et al. 2005; 23) Dudik et al. 2005; 24) Soria et al. 2006a,b; the nuclear X-ray source in VCC1297 has a soft spectrum. However, a thermal model provides a statistically worse fit that a power law model (employing Cash statistics), implying that most of the X-ray emission is likely accretion-powered.

a) Archival data; b) From  $B_T$  magnitude in Ferrarese et al. (2006b); c) The X-ray source appears slightly elongated;  $L_{\text{X,nucl}}$  is estimated within the *Chandra* PSF at 1.5 keV.

The threshold energy  $E_t$  was derived as follows. As a first step, we extracted the spectrum of the total diffuse emission over a circular aperture of 150'' centered on the galaxy nucleus and excluding all the resolved point sources detected by *wavdetect*. The background for this spectrum was extracted on the S3 chip as far away as possible from the galaxy, using an annulus of inner and outer radius 250'' and 300'', respectively (masking out the resolved X-ray sources). We analyzed the extracted spectra with XSPEC version 11.2.0 (Arnaud 1996), using a combination of optically thin thermal emission for the diffuse gas plus a non-thermal component (power-law model) to represent the emission from the unresolved point sources, under the assumption that the hard spectral component seen in the diffuse emission is mainly due to the contribution of unresolved low-mass X-ray bina-

ries (LMXBs). We fixed the power-law photon index  $\Gamma$  of the hard component due to unresolved LMXBs to the value measured for the cumulative spectrum of all the resolved X-ray sources ( $\Gamma = 1.6$ –1.9). As a model for the diffuse thermal emission, we employed the Astrophysical Plasma Emission Code (APEC) thermal-emission model (Smith et al. 2001) in its most recent version (*vaptec*), which includes a wealth of accurate atomic data. The abundances of neon, magnesium, silicon, and iron were left free to vary. The two spectral components are subjected to a common absorption ( $N_H = 2.5 \times 10^{20} \text{ cm}^{-2}$ ). As a consistency-check, we also re-run the fits by letting both the  $N_H$  column and the power law photon index vary, and recovered the same parameters, within errors.

The fits yielded the temperature of the hot thermally-emitting gas,  $kT_g$ , for each galaxy, and allowed us to esti-

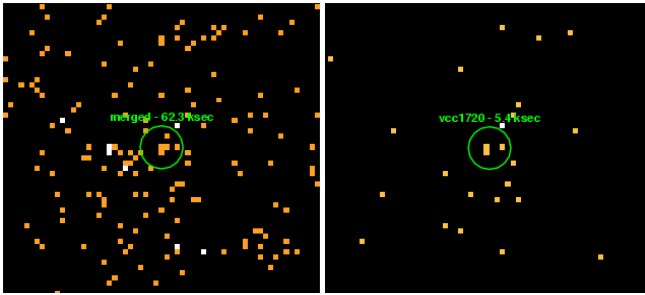


FIG. 2.— The stacked ACIS-S image (left panel) of the 12 out of 16 galaxies which have snapshot (5.4 ksec) observation and no nuclear detection is compared to the image of a single snapshot (VCC1720, right panel). 5 photons are detected within a  $2''$  radius circular aperture center on the stacked nuclear position (green circle), while 3.1 photons are expected from the background over the same area; this implies no significant detection.

mate the energy  $E_t$  above which the optically thin thermal emission contributes to less than 5 per cent to the measured flux. As an example, the 0.3–7 keV spectrum of the diffuse emission of VCC1978(=N4649) is best-fit by a two component model with total flux of  $2.99 \times 10^{-12}$  erg cm $^{-2}$  s $^{-1}$ . The absorbed thermal component accounts for 69 per cent of this flux, but contributes to less than 5 per cent above  $E_t = 1.92$  keV. In this case, the fitted gas temperature is  $kT_g = 0.78^{+0.01}_{-0.02}$  KeV. As in the analysis of the new data described in § 3.1, we converted the measured count rates ( $E_t$ –7 keV) extracted from a  $2''$  circular region centered at the optical nucleus into 0.3–10 keV unabsorbed luminosity within *webPimms*, by assuming an absorbed power law model with photon index  $\Gamma = 2$ . We extracted and fitted the actual source spectrum when dealing with more than 50 hard ( $> E_t$ ) photons (i.e. for VCC1613=M87, VCC1632=N4552, obtaining  $\Gamma = 2.21 \pm 0.04$ ,  $\Gamma = 1.7^{+0.8}_{-0.5}$  respectively).

### 3.3. Hubble Space Telescope imaging

Images from the ACS Virgo Cluster Survey (Côté et al. 2004) were downloaded from the HST archive. The observations of each galaxy consist of two 375s exposures in the F475W filter (nearly equivalent to SDSS  $g'$ -band, effective wavelength  $\lambda_{\text{eff}}=4825$  Å; Fukugita et al. 1996), two 560s exposures in the F850LP filter (nearly equivalent to SDSS  $z'$ -band,  $\lambda_{\text{eff}}=9097$  Å; Fukugita et al. 1996), and a single 90s exposure in the F850LP filter, all in the wide field channel. In order to facilitate the best possible matching between X-ray and optical sources, the astrometry of HST images has been referenced to the that of SDSS-DR5 according to the following procedure. First, individual exposures in each band are combined using the PYRAF task *multi-drizzle*, which includes cosmic ray rejection and correction of geometric distortion. Detection images are built by producing a surface brightness profile of the galaxy using either the PYRAF tasks *ellipse* and *bmodel* or *GALFIT* (Peng et al. 2002), as appropriate. The surface brightness profile and best fit Sersic models contain interesting information on the presence and luminosity of stellar nuclei (see Ferrarese et al. 2006b). The model galaxy is then subtracted and object detection is performed using *SExtractor* with a threshold of 10 connected pixels at a level of  $10\text{-}\sigma$ . Then, a catalog from SDSS is produced using the SDSS-DR5

on-line search tool<sup>8</sup> to retrieve all objects within a radius of  $5'$  of the galactic nucleus. A matching program then determines the coordinate offsets between the two catalogs by applying a Hough transform: first, objects in each catalog are uniquely matched to their nearest neighbor in the opposite catalog and the offset between each pair of objects is calculated; any remaining unmatched objects are discarded. Next, statistics on the offsets in RA and Dec are gathered by an initial pass through all object pairs. Finally, successive rounds of sigma clipping are performed to discard outliers and spurious detections, leaving a minimum of 10 pairs of matched objects from which the overall RA and Dec offsets are calculated. Observed offsets range from  $0'.01 - 1'.2$ , with errors  $0'.01 - 0'.07$ . Offset values are confirmed by manually comparing coordinates of stars and/or galactic nuclei in the ACS images to the SDSS database. No rotation of the world coordinate system is required, as the residual r.m.s. scatter is much smaller than the uncertainty on the position of the X-ray sources, which is dominated by the Chandra PSF and the small number of counts for faint nuclear sources.

Published measurements by the ACSVCS group (Ferrarese et al. 2006b) were used to estimate the B-band luminosity and stellar mass of the host galaxies. Synthetic Vega B-band magnitudes (hereafter B) were obtained from the total (i.e. as obtained from model fitting), extinction-corrected  $g_0$  and  $z_0$  band AB magnitudes, using a broad range of stellar population models (Bruzual & Charlot 2003) to compute the transformation to first order in the color term. We find the transformation to be:

$$B = g_0 + 0.193 + 0.026(g_0 - z_0) \quad (2)$$

Since the B band is close in wavelength to the  $g_0$  band, the transformation introduces only a minimal uncertainty of order 0.01–0.02 mag. The resulting B magnitudes listed in Table 2 typically supercede the photographic  $B_T$  magnitudes (see Côté et al. 2004, and references therein) and, unless otherwise indicated, will be used throughout this series (although for VCC1030 and VCC1535, the  $B_T$  magnitudes are retained since HST photometry was not available). For all the objects with HST photometry, stellar masses were estimated from the  $g_0$  and  $z_0$  band AB model magnitudes using the recipe of Bell et al. (2003):

$$\log(M^*/L_{g_0}) = 0.698(g_0 - z_0) - 0.367 \quad (3)$$

This recipe – and its use of the HST photometry – was found to be more robust than similar ones that use the 2MASS K-band data listed in Ferrarese et al. (2006b), perhaps due to the difficulty of measuring fluxes of the lowest mass galaxies, or with matching the measurement apertures between different types of observation. For the two objects with no HST photometry, we use  $B_T$  and K-band magnitudes and the coefficients provided in Bell et al. (2001) to compute:

$$\log(M^*/L_B) = 0.591(B_T - K) - 1.743 \quad (4)$$

which in these cases gives stellar masses that sit well with objects of comparable luminosity and measured with HST. As noted by Bell et al, the mass to light ratios

<sup>8</sup> <http://cas.sdss.org/dr5/en/tools/search/radial.asp>



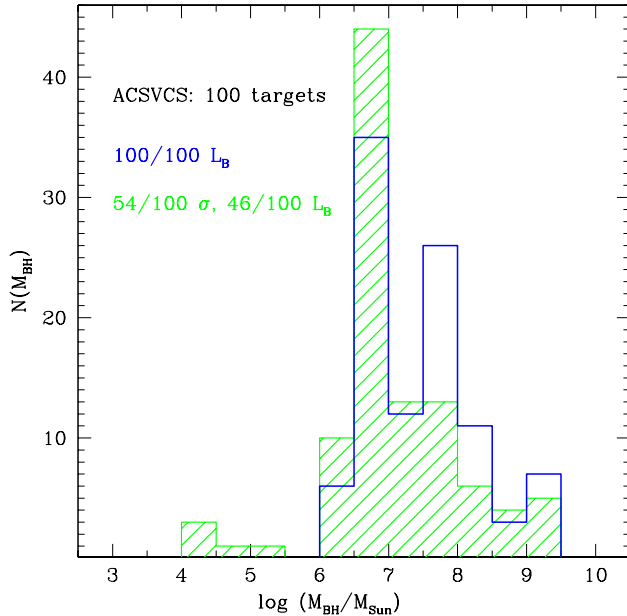


FIG. 3.— Distribution of  $M_{\text{BH}}$  for the 100 spheroids belonging to the ACS Virgo Cluster Survey sample, adopting different mass estimators based on the properties of the host galaxies:  $M_{\text{BH}}\text{-}L_{\text{B}}$  for all galaxies (blue line), and  $M_{\text{BH}}\text{-}\sigma$  for the galaxies with ‘secure’ (see § 4)  $\sigma$  and  $M_{\text{BH}}\text{-}L_{\text{B}}$  otherwise (green shaded). The latter is the fiducial distribution adopted in this paper. Scalings are from Ferrarese & Ford (2005).

calculated with these recipes have systematic uncertainties of some 0.2 dex arising from the assumed initial mass function (a Salpeter function was used in the derivation of the coefficients used here).

#### 4. BLACK HOLE MASSES

In order to construct the distribution of Eddington ratios for our sample, we first need to estimate the masses of the (putative) SMBHs; throughout this Section, we shall *assume* that a SMBH exists at the center of every galaxy in the sample; this working hypothesis will be tested and discussed in § 5.

Although bulge stellar velocity dispersion is arguably the best estimator of  $M_{\text{BH}}$  (e.g. Bernardi et al. 2007), there is considerable interest in comparing  $\sigma$ -based estimates with other estimates. For the most luminous galaxies, such as brightest cluster galaxies,  $\sigma$  and optical luminosity ( $L_{\text{B}}$ ) predict different  $M_{\text{BH}}$  (Lauer et al. 2007a) pointing towards a break down of at least one of the two scaling relations or to a departure from a simple power law. Under the assumption that a SMBH exists at the center of each targeted galaxy, in the following we compare the  $M_{\text{BH}}$  values obtained by employing different empirical scaling relations, specifically the mass-bulge luminosity ( $M_{\text{BH}}\text{-}L_{\text{B}}$ ) or the mass-dispersion velocity ( $M_{\text{BH}}\text{-}\sigma$ ) relation. Unless otherwise indicated, we will employ the scalings given by Ferrarese & Ford (2005; FF05 hereafter).

Velocity dispersions are available in the literature for 74 out of the 100 targets belonging to the ACSVCS, from a variety of sources. In this work we make use of a compilation kindly provided by Lauren MacArthur (MacArthur et al. 2007). However, as black hole mass is a steep function of stellar velocity dispersion, imprecise or inaccurate spectroscopic measurements could introduce significant uncertainty and bias to the black hole

mass estimates. After considering different velocity dispersion values from 12 different sources in literature, and investigating the instrumental resolutions and S/N ratios of the original measurements, a subset of high quality velocity dispersions was identified, yielding a ‘secure’ sub sample of 54 galaxies (see MacArthur et al. 2007 for details).

Figure 3 illustrates the  $M_{\text{BH}}$  distribution of the entire ACSVCS sample as obtained using the two different mass tracers:  $L_{\text{B}}$ -based masses (blue histogram) tend to be higher than  $\sigma$ -based masses (green shaded histogram), particularly at the low-luminosity and low-mass end. While this is a known fact (e.g. Bernardi et al. 2007), in this specific case it can be due to a combination of underestimated  $\sigma$ , overestimated bulge luminosity  $L_{\text{B}}$  (because of low bulge fraction), as well as different slopes of the  $M_{\text{BH}}\text{-}L_{\text{B}}$  and  $M_{\text{BH}}\text{-}\sigma$  relations. Irrespectively of the chosen tracer, however, the distribution of the ACSVCS sample peaks below  $10^7 M_{\odot}$ , where very few direct  $M_{\text{BH}}$  measurements are available.

Studies of active galaxies indicate that the  $M_{\text{BH}}\text{-}\sigma$  relation extends down to the masses probed by our sample (Barth, Greene & Ho 2005), supporting our working hypothesis that  $\sigma$  provides the best estimate of  $M_{\text{BH}}$ . Therefore, the results presented in the rest of the paper will be based on this ‘secure’ sample of stellar velocity dispersions (for 54/100 targets), and on  $L_{\text{B}}$  for the remaining targets. This fiducial  $M_{\text{BH}}$  distribution adopted in this paper is shown in Figure 3 as a green shaded histogram; making use of  $\sigma$  values introduces a minor correction at the low-mass end. Black hole masses based on this secure sample are further compared to  $L_{\text{B}}$ -based  $M_{\text{BH}}$  for different morphological types in the right panel of Figure 4. While a full discussion on the comparison between different  $M_{\text{BH}}$  tracers is beyond the scope of this paper, the plots show that – although the mismatch is reduced when considering only high quality  $\sigma$  – it is present even for pure ellipticals and thus cannot be explained entirely with varying bulge fraction, pointing instead towards a genuine breaking-down of at least one of the two scaling relations at the low mass end. The conclusions of this paper are not significantly affected if different scalings/black hole mass indicators are employed (such as Tremaine et al. 2002 or Marconi & Hunt 2003, for  $M_{\text{BH}}\text{-}\sigma$  and  $M_{\text{BH}}\text{-}L_{\text{B}}$ , respectively).

#### 5. RESULTS

Table 2 lists the nuclear X-ray properties for the 32 targets under analysis. We detect point-like X-ray emission from a position consistent with the optical nucleus in 16 targets, 4 of which (VCC2092, VCC1692; VCC1883, VCC1178) belong to the list of new snapshot (5.4 ksec) *Chandra* observations. A montage of the ACIS-S images of the detected nuclei is shown in Figure 5. For the 16 targets with archival data, we were able to compare our results on the nuclear X-ray sources (or lack thereof) with the literature in 11 cases, finding good agreement with the published values: after re-scaling to the same distances, we obtain an average luminosity difference of 0.03 dex, with a scatter of 0.17 dex. No fluxes/upper limits had been published for the nuclear emission for the remaining 5 targets. We briefly comment on them below. VCC1903: the *Chandra* data for this galaxy have been analyzed and discussed in a number of publications,

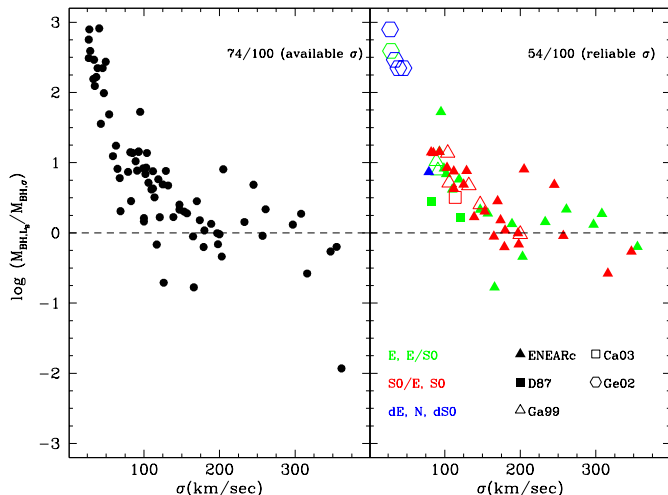


FIG. 4.— *Left*: Ratio of  $M_{\text{BH}}$  as estimated from the  $M_{\text{BH}}-\sigma$  relation to that estimated from the  $M_{\text{BH}}-L_{\text{B}}$  relation (both scalings are from FF05) for the 74 targets for which  $\sigma$  measurements are available in the literature. *Right*: Same as left, only for the 54 objects with ‘secure’  $\sigma$  measurements. Here, targets are color-coded for different morphological types, showing that the discrepancy at the low-mass/low-luminosity end cannot be entirely due to a reduced bulge fraction. References are: Bernardi et al. (2002; ENEARc); Davis et al. (1987; D87); Gavazzi et al. (1999; Ga99); Caldwell et al. (2003; Ca03) and Geha et al. (2002; Ge02).

focusing either on the diffuse X-ray emission properties or the X-ray binary population. VCC881, VCC1535: the data for these galaxies have been discussed in the context of X-ray binary population studies, excluding the central regions (e.g. Sivakoff et al. 2007). VCC1231, VCC2095: no publication has been found regarding these *Chandra* datasets.

A fundamental point to be addressed is the nature of the detected nuclear X-ray emission. In principle, hard X-rays provide us with some clear-cut diagnostics for accretion-powered emission, as a result of non-thermal processes such as Comptonization. In particular, here we ask the question whether accretion-powered emission from a SMBH is at the origin of the detected nuclear sources. In the following, we shall carefully address the issue of contamination from background X-ray sources as well as low mass X-ray binaries (§ 5.1), which are the major source of concern. This is closely related to the issue of whether SMBHs exist and/or they are *detectable* at the center of faint spheroids which may host compact stellar clusters (§ 5.2). The Eddington distribution of the detected nuclei is presented in § 5.3, and discussed in the context of the various model for inefficient accretion and mechanical feedback from SMBHs.

### 5.1. Origin of the detected X-ray emission

We argue that the detection of point-like X-ray emission from a position coincident with the optical nucleus is unlikely to be due to any process other than accretion onto a nuclear SMBH. Based on the results by Rosati et al. (2002), we estimate that the chance of detecting a background X-ray source within the *Chandra* PSF at 1.5 keV (convolved with the positional uncertainty) is lower than  $10^{-6}$ . Hence, the most likely contamination arises from LMXBs. In a broad stellar mass range, *and in the absence of a nuclear star cluster* (see § 5.2), the total number of LMXBs and their cumulative X-ray

luminosity are proportional to the stellar mass of the host galaxy,  $M_*$  (Gilfanov 2004; Kim & Fabbiano 2004; Humphrey & Buote 2006). The number  $n_X$  of expected sources per unit stellar mass above a certain luminosity threshold can be estimated from the X-ray luminosity function for LMXBs (e.g. Gilfanov 2004). In turn, the number of expected sources within the *Chandra* PSF (convolved with the positional uncertainty) is given by  $n_X$  times  $M_{*,\text{PSF}}$ : the stellar mass within the central aperture. We estimated  $M_{*,\text{PSF}}$  for each galaxy from the archival ACS images, adopting the same procedure as described in § 4. The number of expected LMXBs above the X-ray luminosity of the detected nuclei turns out to be typically lower than a few  $10^{-2}$  for the most massive galaxies (which do not harbor prominent stellar clusters at the center; Ferrarese et al. 2006b). High mass X-ray binaries are not expected to contribute in early-type galaxies, where star formation is nearly absent. As an example, the number of expected LMXB with  $L_X > L_{X,\text{nucl}} = 4.7 \times 10^{38} \text{ erg s}^{-1}$  (VCC1178) is about 6 per  $10^{11} M_\odot$  (this is obtained employing the functional shape obtained by Gilfanov 2004 specifically for early-type galaxies). This means that fewer than 0.06 sources as bright/brighter than the detected nucleus are expected within the central aperture, home to  $\sim 9 \times 10^8 M_\odot$ . Given the shape of the LMXB luminosity function at high luminosities (above a few  $10^{38} \text{ erg s}^{-1}$ ), we can also confidently rule out that the central X-ray source is due to a collection of fainter LMXBs, as the integral  $\int n_X \times L_X dL_X$  is dominated by the luminosity term. The same conclusion is reached by Sivakoff et al. (2007) in an extensive study of the X-ray luminosity function of globular clusters in early-type galaxies (see § 5.2). As an example, in the case of VCC1178, the number of expected nuclear LMXBs brighter than 1/10 of the detected nucleus is less than 0.6. However, massive star clusters have been shown to become more and more common at the center of spheroids moving down the mass function (Ferrarese et al. 2006a), and may well increase the chance of harboring bright X-ray binaries. This is further explored in the next Section.

### 5.2. SMBHs in low-mass spheroids

Possibly the most noteworthy result of this study is the detection of nuclear hard X-ray emission from faint early-type galaxies: in particular, two of the detected nuclei are hosted in galaxies with absolute B magnitudes lower than  $-18$ : VCC1178(=N4464) and VCC1297(=N4486B) have  $M_B = -17.68$  and  $M_B = -16.91$ , respectively.

From an observational standpoint, the very existence of SMBHs (of the same sort that define the known scalings in massive galaxies) in faint inactive galaxies remains questionable. Ferrarese et al. (2006a) suggest that the creation of a ‘central massive object’, SMBH or compact stellar nucleus, would be the natural byproduct of galaxy evolution, with the former being more common in massive bright galaxies ( $M_B$  brighter than  $-20$ ), and the latter dominating –possibly taking over– at magnitudes fainter than  $-18$ .

This finds support in semi-analytical models which follow the formation and evolution of black holes seeds formed at high redshift in the context of hierarchical cosmologies. On one side, SMBH formation mechanisms seem to be more efficient in halos of high mass; on the



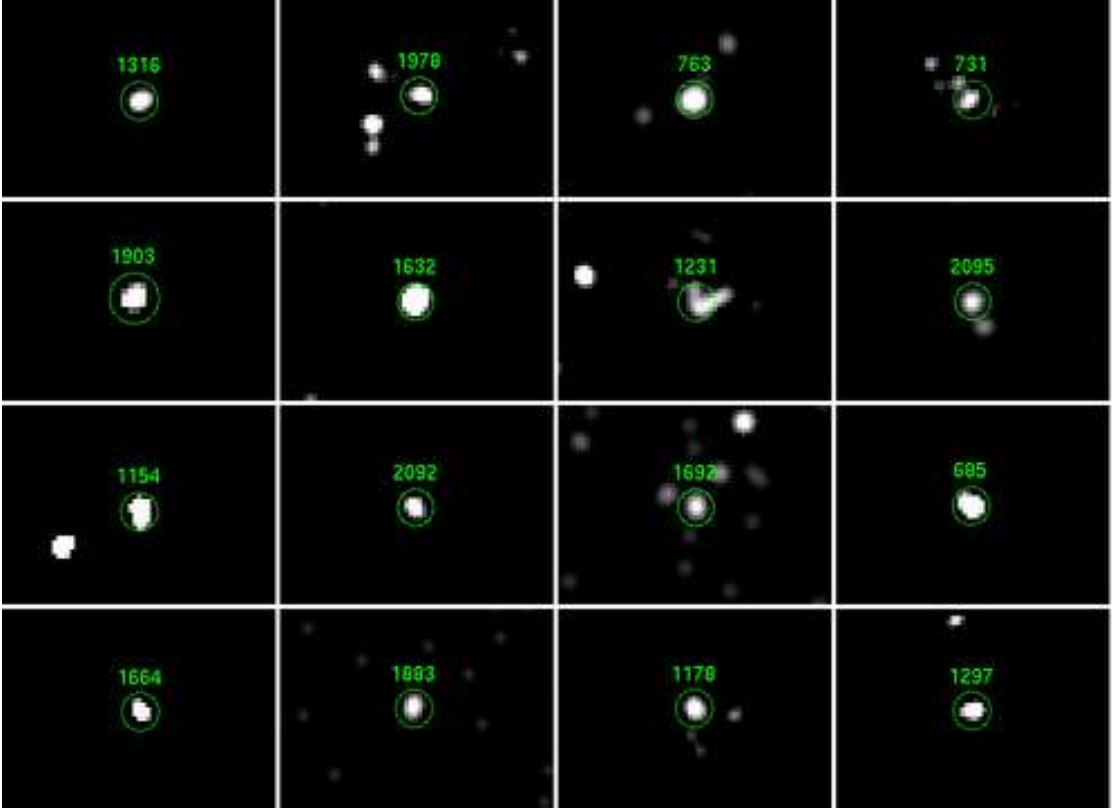


FIG. 5.— *Chandra* ACIS-S images of the 16 detected X-ray nuclei, smoothed with a Gaussian of  $\sigma=3''$ . The green circle represent the count extraction region, centered on the *wavdetect* centroid. Four of the detected targets belong to the large program survey and were observed during Cycle 8 (VCC2092, VCC1692, VCC1883, VCC1178); three targets have archival observations but no literature reference for the nuclear source (VCC1903, VCC1231, VCC2095). The faintest detection, both in terms of nuclear X-ray luminosity and host galaxy magnitude ( $M_B=-16.85$ ), is VCC1297, and was previously reported by Soria et al. (2006b).

other, low-mass objects are more likely to eject their nuclear SMBH following a major merger as a result of gravitational recoil. The combination of these two effects may lead to a lower black hole occupation fraction in low mass galaxies at red-shift zero (Volonteri et al. 2007a,b; it should be stressed however, that in this scenario nuclear SMBHs and compact star clusters are not necessarily mutually exclusive). Observationally, the fraction of X-ray detectable SMBHs (assuming that they can indeed be distinguished from bright LMXBs) would naturally place a lower limit on the black hole occupation fraction in low-mass spheroids. We investigate this below.

As shown in Figure 6, VCC1178 and VCC1297 do not have a particularly prominent nuclear star cluster, consistent with the findings of Ferrarese et al. (2006b). However, the case for a SMBH is quite strong in VCC1297(=N4486B): based on data from the Wide Field Planetary Camera 2 (WFPC2), Lauer et al. (1996) showed evidence for a central double nucleus in this galaxy; subsequently, based on stellar kinematics studies, Kormendy et al. (1997) derived a nuclear ‘dark mass’ of  $6 \times 10^8 M_\odot$ , both arguing in favour of a nuclear SMBH. A small excess with respect to the model fit in the inner region of the profile is just noticeable in VCC1178. We note however that this conclusion is highly dependent upon the assumed form of the profile of the underlying faint galaxy, which has no fundamental reason to follow exactly a Sersic-law. In fact, Lauer et al. (2007b) performed deconvolved HST ACS surface

photometry study of a sample of early-type galaxies, including VCC1178(=N4464), and found evidence for a nuclear source in this system by modeling the profile with a Nuker law. Assuming that the excess flux is due to a nuclear star cluster in this galaxy, we estimate its luminosity to be approximately  $2.8 \pm 0.3 \times 10^7 L_{\odot,z}$ , where the error bar is the semi-difference of the results obtained from two different methods that should bracket the true answer: i) fitting a point spread function + Sersic model; ii) aperture photometry on the residuals of the Sersic fit within a  $0''.5$  radius aperture. This corresponds to a stellar mass between  $3.7 - 4.6 \times 10^7 M_\odot$ , where we have adopted a mass-to-light ratio  $\Upsilon_z = 1.45$ , to ensure a proper comparison with the work by Sivakoff et al. (2007), which provides an expression for the expected number of bright LMXBs specifically in globular clusters (rather than averaged over the entire galaxy).

It is known that, while hosting a small percentage of the galaxy stellar mass, globular clusters are home to about 50 per cent of the observed LMXBs. In this environment, the number of expected LMXB sources scales non-linearly with the cluster mass (Sivakoff et al. 2007); this also leads to the prediction that high X-ray luminosity clusters (with super-Eddington luminosities for  $3 M_\odot$ ) contain a *single LMXB*. Sivakoff et al. (2007) derive an expression for the expected number  $n_X$  of LMXBs brighter than  $3.2 \times 10^{38} \text{ erg s}^{-1}$  (the luminosity limit is set by the sample completeness) in a star cluster of stellar

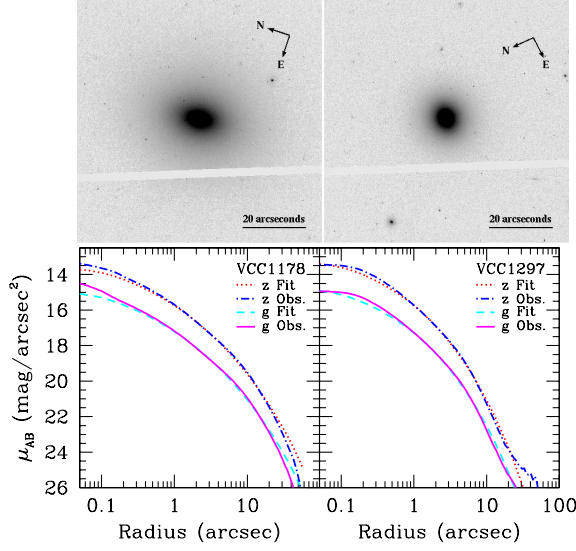


FIG. 6.— *Upper panels:*  $g'$ -band HST images of VCC1178 (left) and VCC1297 (right), as observed in the ACS Virgo Cluster Survey (Côté et al. 2004). The field of view is approximately  $72''$  on a side. *Lower panels:* azimuthally averaged  $g'$  (solid magenta) and  $z'$ -band (dashed-dotted blue) surface brightness profiles for VCC1178 and VCC1297 (the actual errorbars are too small to be visible on the plots). Best-fit single-component Sersic models (cyan and red) are over-plotted for each galaxy. A nuclear cusp is just visible in the inner  $\sim 0''.2$  of the VCC1178 profile, in contrast to the flattened nuclear profile observed in VCC1297.

mass  $M$ , half mass radius  $r_{h, \text{corr}}$ , and color ( $g-z$ ):

$$n_X = 8 \times 10^{-2} (M/10^6 M_\odot)^{1.237} 10^{0.9(g-z)} (r_{h, \text{corr}}/1 \text{ pc})^{-2.22} \quad (5)$$

where  $r_{h, \text{corr}} = r_h \times 10^{0.17[(g-z)-1.2]}$ . An estimate of the half mass radius of the star cluster in VCC1178 is obtained by measuring the light in the residuals as a function of photometric aperture, and varies between 25 and 30 pc. Together with the fitted luminosities, this implies  $n_X = 0.06-0.12$  (obtained by adopting the fitted parameters with method i) and ii), respectively). The expected number of LMXBs in a globular cluster can be converted to a probability  $P_X$  that there is at least one LMXB brighter than the adopted X-ray luminosity threshold assuming a Poisson distribution:  $P_X \lesssim 0.11$  (95 per cent confidence).

We note that this value represents a conservative estimate of the actual probability contamination, in that it is estimated for a LMXB X-ray luminosity threshold lower than any of the detected nuclei in our sample. In addition, LMXBs are found more often in globular clusters with smaller half-mass radii: since there is no correlation between the half-mass radius and the mass in globular clusters (e.g. Jordán et al. 2005), this simply implies that LMXBs are found more often in *denser* environments, with higher encounter rates (Sivakoff et al. 2007). The inferred half-mass radius of the (possible) nuclear star cluster in VCC1178 (20-30 pc) is much higher than the typical radius estimated for standard globular clusters (few pc, with a median value of 2.2 pc in the work by Sivakoff et al. ). From this, we conclude that a bright LMXB is unlikely to be at the origin of the observed nuclear emission in VCC1178, with a maximum chance contamination of 11 per cent.

The incidence of X-ray ‘active’ (hereafter defined as detected in the X-ray band down to our luminosity thresh-

old of  $\sim 4 \times 10^{38} \text{ erg s}^{-1}$ ) SMBHs as a function of the host galaxy stellar mass,  $M_*$ , is illustrated in the upper panel of Figure 7. Splitting the sample in two mass bins, above and below a stellar mass threshold of  $10^{10} M_\odot$ , and by making use of binomial statistics applied to small number of observed events (Gehrels 1986) we are able to conclude that *the incidence of nuclear X-ray super-massive black hole activity – down to our completeness limit of  $\sim 4 \times 10^{38} \text{ erg s}^{-1}$  – increases with the stellar mass of the host* (see Figure 7, lower panel). Specifically: between 3 and 44 per cent of the galaxies with stellar masses  $< 10^{10} M_\odot$  are found to host an active SMBH (2 out of 12). The incidence of nuclear activity increases to between 49 and 87 per cent in galaxies with stellar masses above  $10^{10} M_\odot$  (14 out of 20 are active; percentages are given at the 95 per cent confidence level). For comparison, in a recent comprehensive optical spectroscopic census of nuclear activity associated with *late*-type galaxies in Virgo, Decarli et al. (2007) find no AGN in galaxies with dynamical mass lower than  $10^{10} M_\odot$  (in that work, line ratios are adopted in order to classify/distinguish AGN from transition objects and/or HII regions, specifically:  $N_{\text{II}}/H_\alpha > 0.6$  unambiguously identifies AGN).

### 5.3. Eddington-ratio distribution and nuclear SMBH feedback

Having shown that point-like nuclear X-ray emission is likely due to accretion onto a SMBH – and under the assumption that the sample galaxies all host a SMBH whose mass obeys the known scaling relations defined by SMBHs in massive bright galaxies – we can construct the  $L_X/L_{\text{Edd}}$  distribution of our sample, shown in Figure 8 by adopting the fiducial black hole mass distribution described in § 4.

For any plausible value of the bolometric correction  $f_{\text{bol}} = L_{\text{bol}}/L_X$  (which may vary between  $\sim 8$  and  $\sim 60$ ; Marconi et al. 2004), the detected nuclei are highly sub-Eddington. Under the conservative assumption that only as little as 2% of accretion-driven emission is emitted in the X-ray band, the inferred  $L_{\text{bol}}/L_{\text{Edd}}$  ratios do not exceed  $10^{-4.7}$  for this sub-sample (inferred for VCC1883, the highest  $L_X/L_{\text{Edd}}$  nucleus among our 16 snapshot observations). Similarly, the upper limit to the *average* X-ray luminosity in the stacked image of the 12 undetected-nuclei with snapshot observations (Figure 2, left panel) amounts to  $3.8 \times 10^{37} \text{ erg s}^{-1}$ , or  $(L_X/L_{\text{Edd}}) \lesssim 3 \times 10^{-8}$ , over 0.3-10 keV for an average black hole mass of  $9.3 \times 10^6 M_\odot$ . Similar results are obtained by Santra et al. (2007) for a sample of 13 early-type galaxies in the core of the Perseus cluster with a deep *Chandra* exposure, as well as from Soria et al. (2006a) and Pellegrini (2005). Following their approach (see eqs. 4 and 5 in Soria et al. 2006a), we can compare the measured X-ray luminosities to the bolometric accretion power  $L_{\text{acc, IS}}$  expected from Bondi accretion of the interstellar medium:  $L_{\text{acc, IS}} = \eta \dot{M}_B c^2$ , where the radiative efficiency  $\eta$  is a fraction  $f_r$  of the total accretion efficiency  $\eta'$ , and  $\dot{M}_B$  – the Bondi accretion rate – can be expressed as:

$$\dot{M}_B = 1.6 \times 10^{-5} \left( \frac{M_{\text{BH}}}{10^8 M_\odot} \right)^2 \left( \frac{0.5 \text{ keV}}{kT} \right)^{3/2} \times \left( \frac{n_0}{0.01 \text{ cm}^{-3}} \right) M_\odot \text{ yr}^{-1}, \quad (6)$$

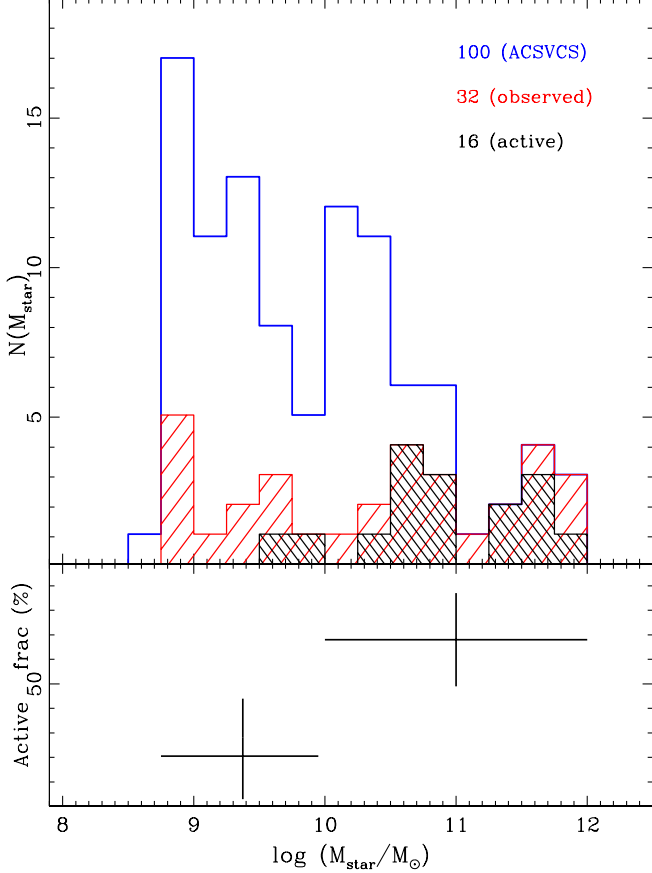


FIG. 7.— *Upper panel*: Stellar mass distribution of the early-type galaxies belonging to the ACSVCS sample (blue histogram). The distribution of the 32 targets considered in this work is shown as a red shaded histogram. The distribution of the 16 targets with an X-ray active SMBH at the center is represented by a black double-hatched histogram. Galaxy stellar masses  $M_*$  are estimated based on their B-band luminosity and colors, as described in § 3.3. Two of the detected nuclei (VCC1178=N4464 and VCC1297=N4486B) belong to galaxies with stellar mass lower than a few  $10^{10} M_\odot$ , where the very survival (or existence) of SMBH has been questioned (see Figure 6 and discussion in § 5.2). *Lower panel*: incidence of X-ray nuclear activity as a function of the host stellar mass. Only 2 out of the 12 galaxies with stellar mass below  $10^{10} M_\odot$  host an active SMBH, i.e. between 3–44 per cent. The percentage raises to 49–87 per cent above  $10^{10} M_\odot$ , where 14 out 20 galaxies host an active nuclear SMBH (numbers are given at the 95 per cent confidence level).

being  $T$  and  $n_0$  the temperature and density of the hot interstellar gas ( $k$  is the Boltzmann constant). Adopting conservative values of  $0.01 \text{ cm}^{-3}$  for  $n_0$  (in order to minimize  $L_{\text{acc,IS}}$ ) and for the range of temperatures which we infer for the hot gas (§ 3.2), we obtain:

$$\frac{L_X}{0.1\dot{M}_B c^2} = f_X f_r \left( \frac{\eta'}{0.1} \right) \left( \frac{\dot{m}}{\dot{m}_B} \right) \sim 2 \times 10^{-5} - 0.6, \quad (7)$$

where  $f_X = 1/f_{\text{bol}}$  ( $0.02 \lesssim f_X \lesssim 0.12$ ; Marconi et al. 2004),  $\dot{m}$  and  $\dot{m}_B$  are Eddington-scaled  $\dot{M}$  and  $\dot{M}_B$ , respectively, and  $c$  is the speed of light. All the detected nuclei in the AMUSE-Virgo sub-sample presented here are under-luminous with respect to Bondi accretion from the interstellar medium.

The accretion mode responsible for powering low-luminosity black holes is still a matter of debate. Observations of highly sub-Eddington black holes, most notably the Galactic Center Sag A\*, paved the way

to radiatively inefficient accretion flow models (RIAFs). Advection-dominated accretion flows (ADAFs; Ichimaru 1977; Narayan & Yi 1994) are popular analytical models for the dynamics of RIAFs at low accretion rates. However, they face a number of difficulties. In particular, Blandford & Begelman (1999; 2004) argued that the accreting gas in an ADAF is generically unbound and free to escape to infinity, and elaborated an alternative model, named the adiabatic inflow outflow solution (ADIOS). Here the key notion is that the excess energy and angular momentum is lost to a wind at all radii; the final accretion rate into the hole may be only a tiny fraction of the mass supply at large radii. This is a generalization of and an alternative to an advective inflow. Deep *Chandra* observations of nearby massive ellipticals (Allen et al. 2006), have shown that a tight, almost linear, correlation exists between the Bondi accretion rate and the jet kinetic power (measured from the  $p \times dV$  work exerted on X-ray cavities). The correlation implies that a substantial fraction of the energy associated with gas entering the Bondi radius must be dissipated mechanically, via jets/outflows.

This is closely related to the role of SMBH feedback in galaxy evolution (see e.g. McNamara & Nulsen 2007). Semi-analytical models applied to dark matter simulations for the growth and evolution of cosmic structures have recently emphasized the role of *mechanical*, rather than radiated, SMBH feedback. A prolonged phase of low-level accretion, resulting in sub-Eddington luminosities, proves to be effective at quenching star formation. It is worth stressing though, that in this formulation SMBH feedback plays a role in the most massive bright galaxies only: once star formation has halted, these massive red galaxies continue to grow through merging. This allows the brightest cluster galaxies to gain a factor of 2 or 3 in mass without significant star formation. However, it is not clear whether such a mechanism might switch off at or be still important at low-masses. Merloni & Heinz (2007) have addressed this issue of mechanical SMBH feedback by comparing a sample of 15 sub-Eddington nuclei for which information on the Bondi rate, kinetic power, and radiative power is available. For these objects, they find that the Eddington-scaled black hole kinetic power,  $L_{\text{kin}}$  (which is a proxy for  $L_{\text{BH}}$  – the SMBH power feedback – in the formalism of Croton et al. 2006) scales with the nuclear X-ray luminosity (2–10 keV) according to the following relation:

$$\log(L_{\text{kin}}/L_{\text{Edd}}) = 0.49 \log \lambda_X - 0.78 \quad (8)$$

where  $\lambda_X = 5 \times L_{(2-10 \text{ keV})}/L_{\text{Edd}}$  (with a scatter of 0.39 dex).

Applying the Merloni & Heinz scaling to our sample (where with are arbitrarily assuming that the same correlation applies to lower-mass, lower-luminosity objects spheroids<sup>9</sup>), the measured X-ray luminosities translate into Eddington-scaled kinetic luminosity in the range  $\sim 10^{-3}$  (VCC1664) to  $\sim 10^{-5}$  (VCC1978), which suggest that energy feedback might be effective even in low mass spheroids.

## 6. SUMMARY AND CONCLUSIONS

<sup>9</sup> In fact 4 out of 32 objects in our sample belong to the sample examined by Merloni & Heinz.

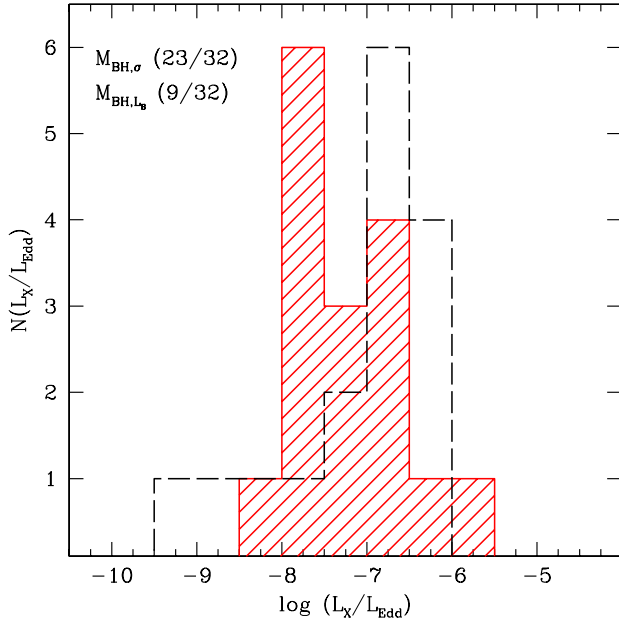


FIG. 8.—  $L_X/L_{\text{Edd}}$  (0.3–10 keV) distribution of the 32 targets under analysis. Black hole masses are calculated from dispersion velocities  $\sigma$  when deemed ‘secure’ (for 23/32 targets), from  $L_B$  otherwise. The red histogram represents the 16 detections, the dotted line represents luminosity upper limits.  $L_X$  is measured between 0.3–10 keV. *Bolometric* luminosities are likely a factor 8–60 higher (based on Marconi et al. 2004).

This paper presents the first *Chandra* results of AMUSE-Virgo, a multi-wavelength survey of early type galaxies in the Virgo cluster, aimed at investigating the incidence and activity of super-massive black holes in the nuclei of 100 local nearby spheroids. The ACSVCS sample (Côté et al. 2004) is selected based on the properties of the host galaxies, and therefore it is an unbiased census of nuclear activity as a function of host galaxy stellar mass (and hence presumably black hole mass). Since the stellar mass distribution of the galaxies peaks below  $10^{10} M_\odot$ , AMUSE-Virgo will provide us the deepest census of low-level accretion-powered activity in early type galaxies over an unprecedented range of masses. In this paper, we combine *Chandra* results from the first 16 targets with the analysis of archival data of 16, typically more massive, targets. The absolute B magnitudes of this sample of 32 objects range from  $M_B = -22.5$  to  $M_B = -15.0$ .

The main results of this study can be summarized as follows:

- We detect point-like X-ray emission from a position consistent with the optical nucleus in 50 per cent of the targets. 12 detection out of 16 belong to the archival observations, but only 9 out of those 12 were previously reported in the literature. The remaining 4 detections (VCC2092, VCC1692, VCC1833, VCC1178) were made using new snapshot observations of low-mass targets.
- Two of the detected nuclei (VCC1178 and VCC1297, having  $L_X = 4.7 \times 10^{38}$  and  $2.6 \times 10^{38}$  erg s $^{-1}$ , respectively) are hosted in galaxies with absolute B magnitude fainter than  $-18$  ( $M_B = -17.68$  and  $-16.91$ ), or host galaxy stellar mass lower than  $10^{10} M_\odot$  ( $M_\star = 8.1 \times 10^9 M_\odot$  and  $5.1 \times 10^9 M_\odot$ ). At these luminosities, massive stellar clusters are

known to become increasingly common, and have been suggested to possibly even replace SMBHs (of the kind that define empirical scaling relations at the bright end; Ferrarese et al. 2006a).

- Analysis of archival ACS HST images reveals a slight excess in the surface brightness profile of VCC1178, with respect to a Sersic model. We conservatively interpret this as due to a nuclear star cluster. The inferred stellar mass does not exceed a few  $10^7 M_\odot$ , implying a less than 11 per cent probability that the nuclear X-ray source is a solar mass compact object based on results by Sivakoff et al. (2007).
- After carefully addressing possible contamination from low mass X-ray binaries in the remaining objects (based on the luminosity function by Gilfanov 2004), we conclude that *the nuclear X-ray sources are most likely due to low-level accretion-powered activity from a super-massive black hole*.
- Between 3 and 44 per cent (95 per cent confidence level) of the galaxies with stellar masses lower than  $10^{10} M_\odot$  harbor an X-ray active SMBH – down to our completeness limit of  $\sim 4 \times 10^{38}$  erg s $^{-1}$ . The fraction of galaxies hosting an active SMBH increases to between 49 and 87 per cent for host masses above  $10^{10}$ . Even with only a third of the sample (32/100 galaxies), this study shows that there is *statistically significant increase in the incidence of nuclear activity towards the high mass end*, consistent with what found in late-type Virgo galaxies (Decarli et al. 2007). This should be folded with the actual black hole mass function in order to properly constrain the distribution of nuclear activity.
- The upper limit to the *average* X-ray luminosity in the stacked image of the 12 undetected-nuclei with snapshot (5.4 ks) *Chandra* observations amounts to  $3.8 \times 10^{37}$  erg s $^{-1}$ , or  $\langle L_{(0.3-10 \text{ keV})}/L_{\text{Edd}} \rangle < 3 \times 10^{-8}$  for an average black hole mass of  $9.3 \times 10^6 M_\odot$ .
- Based on ‘fiducial’ values for the central black hole mass (based on ‘secure’ measurements of the dispersion velocity for 24 targets, and on B magnitude otherwise) the ratio  $L_{(0.3-10 \text{ keV})}/L_{\text{Edd}}$  varies between  $10^{-8.4}$  and  $10^{-5.9}$  for the detected nuclei. The detected nuclei are under-luminous with respect to Bondi accretion from the interstellar gas. In agreement with earlier works (e.g. Pellegrini 2005; Soria et al. 2006a,b; Santra et al. 2007), this argues for an inefficient accretion mechanism, albeit our results can not break the degeneracy between intrinsically low radiative efficiency and/or drastically reduced mass accretion rate onto the black hole (owing to outflows/winds).

A crucial question still to be addressed is that of the amount of power released in the form of kinetic energy. According to a recent study by Merloni & Heinz (2007), a (non-linear) correlation exists between the Eddington-scaled kinetic power and the bolometric luminosity. The



non-linearity implies that the relative amount of power dissipated by these nuclei in the form of mechanical power decreases toward low X-ray luminosities. If the same scaling is applied to our sub-sample of 16 detected X-ray nuclei, the inferred kinetic power are between  $\sim 10^{-5} - 10^{-3} L_{\text{Edd}}$ , indicating that low-level SMBH feedback can be effective in faint spheroids as well as in bright massive elliptical galaxies.

Most of the galaxies yet to be observed as part of AMUSE-Virgo have stellar masses around  $10^{9.5} M_{\odot}$ , a mass range that remains largely unexplored as far as low-level nuclear SMBH activity is concerned. *Chandra* observations of 68 additional faint galaxies are under way, and will further constrain the fraction of galaxies that harbor a nuclear X-ray source. As shown by Ferrarese et al. (2006a), massive nuclear star clusters become increasingly common down the galaxy mass function, thereby increasing the chance of bright LMXB contamination. Detection of a high brightness temperature compact radio counterpart to the detected X-ray nuclei would provide definitive evidence for an accreting SMBH, as no Galactic X-ray binary can be possibly detected in the radio band at the Virgo cluster distance with current instrumentation. In fact, with the exception of the known radio sources VCC1226(M49), VCC1316(M87), VCC1978(M60), VCC763(M84), VCC1535(N4526), VCC1632(M89), none of the sample galaxies have a detected radio core brighter than the limiting flux density of 1.8 mJy at 1.4 GHz.<sup>10</sup> At the average distance of 16.5 Mpc, this corresponds to an upper limit to the radio luminosity of  $\nu L_{\nu} < 8.3 \times 10^{38} \text{ erg s}^{-1}$ . Deep radio observations of the targeted nuclei, with the Very Large Array, are in progress, and will put further constraints on the spectral energy distribution at low frequencies. At the same time, while LMXBs are known to emit the bulk of the dissipated accretion power

in the X-ray band, SMBHs typically emit at longer wavelengths, yielding bolometric corrections as high as 80 (Marconi et al. 2004); upcoming mid-IR observations, with the *Spitzer Space Telescope*, will hopefully enable us to estimate the bolometric luminosity of the detected nuclei, and to uncover obscured SMBH activity.

E.G. is supported through *Chandra* Postdoctoral Fellowship grant number PF5-60037, issued by the *Chandra* X-Ray Center, which is operated by the Smithsonian Astrophysical Observatory for NASA under contract NAS8-03060. T.T. acknowledges support from the NSF through CAREER award NSF-0642621, by the Sloan Foundation through a Sloan Research Fellowship, and by the Packard Foundation through a Packard Fellowship. P.J.M. is supported by the TABASGO foundation in the form of a research fellowship. Support for this work was provided by NASA through Chandra Award Number 08900784 issued by the Chandra X-ray Observatory Center. This work is based on data obtained with the Chandra X-ray Observatory and archival data from the Hubble Space Telescope, obtained from the data archive at the Space Telescope Institute, which is operated by the association of Universities for Research in Astronomy, Inc. for NASA under contract NAS5-26555. We are grateful to Lauren MacArthur for sharing with us her compilation of velocity dispersion for Virgo galaxies. We acknowledge stimulating conversations with Luca Ciotti, Darren Croton, Andrés Jordán, Andrea Merloni, Gregory Sivakoff and Marta Volonteri. We thank Andy Fabian and Tod Lauer for useful comments and for pointing out relevant references, and the referee, Silvia Pellegrini, for a detailed and constructive report.

<sup>10</sup> Data based on GOLDMine: <http://goldmine.mib.infn.it/>

## REFERENCES

- Abraham, R. G., Nair, P., McCarthy, P. J., Glazebrook, K., Mentuch, E., Yan, H., Savaglio, S., Crampton, D., Murowinski, R., Juneau, S., Le Borgne, D., Carlberg, R. G., Jørgensen, I., Roth, K., Chen, H.-W., & Marzke, R. O. 2007, *ApJ*, 669, 184
- Allen, S. W., Dunn, R. J. H., Fabian, A. C., Taylor, G. B., & Reynolds, C. S. 2006, *MNRAS*, 372, 21
- Allen, S. W., Di Matteo, T., & Fabian, A. C. 2000, *MNRAS*, 311, 493
- Arnaud, K. A. 1996, 101, 17
- Baganoff, F. K., Maeda, Y., Morris, M., Bautz, M. W., Brandt, W. N., Cui, W., Doty, J. P., Feigelson, E. D., Garmire, G. P., Pravdo, S. H., Ricker, G. R., & Townsley, L. K. 2003, *ApJ*, 591, 891
- Barth, A. J., Greene, J. E., & Ho, L. C. 2005, *ApJ*, 619, L151
- Barth, A. J., Ho, L. C., Rutledge, R. E., Sargent, W. L. W. 2004, *ApJ*, 607, 90
- Begelman, M. C., Volonteri, M., & Rees, M. J. 2006, *MNRAS*, 370, 289
- Bell, E. F., McIntosh, D. H., Katz, N., & Weinberg, M. D. 2003, *ApJS*, 149, 289
- Bell, E. F. & de Jong, R. S. 2001, *ApJ*, 550, 212
- Bernardi, M., Sheth, R. K., Tundo, E., & Hyde, J. B. 2007, *ApJ*, 660, 267
- Bernardi, M., Alonso, M. V., da Costa, L. N., Willmer, C. N. A., Wegner, G., Pellegrini, P. S., Rité, C., & Maia, M. A. G. 2002, *AJ*, 123, 2990
- Billar, B. A., Jones, C., Forman, W. R., Kraft, R., & Ensslin, T. 2004, *ApJ*, 613, 238
- Blandford, R. D. & Begelman, M. C. 2004, *MNRAS*, 349, 68
- Blandford, R. D. & Begelman, M. C. 1999, *MNRAS*, 303, L1
- Bundy, K., Ellis, R. S., & Conselice, C. J. 2005, *ApJ*, 625, 621
- Bruzual, G. & Charlot, S. 2003, *MNRAS*, 344, 1000
- Caldwell, N., Rose, J. A., & Concannon, K. D. 2003, *AJ*, 125, 2891
- Ciotti, L. & Ostriker, J. P. 2007, *ApJ*, 665, 1038
- Ciotti, L., Pellegrini, S., Renzini, A., & D’Ercole, A. 1991, *ApJ*, 376, 380
- Churazov, E., Sazonov, S., Sunyaev, R., Forman, W., Jones, C., & Böhringer, H. 2005, *MNRAS*, 363, L91
- Côté, P., Piatek, S., Ferrarese, L., Jordán, A., Merritt, D., Peng, E. W., Hasegan, M., Blakeslee, J. P., Mei, S., West, M. J., Milosavljević, M., & Tonry, J. L. 2006, *ApJS*, 165, 57
- Côté, P., Blakeslee, J. P., Ferrarese, L., Jordán, A., Mei, S., Merritt, D., Milosavljević, M., Peng, E. W., Tonry, J. L., & West, M. J. 2004, *ApJS*, 153, 223
- Cowie, L. L., Songaila, A., Hu, E. M., & Cohen, J. G. 1996, *AJ*, 112, 839
- Croton, D. J., Springel, V., White, S. D. M., De Lucia, G., Frenk, C. S., Gao, L., Jenkins, A., Kauffmann, G., Navarro, J. F., & Yoshida, N. 2006, *MNRAS*, 367, 864
- Decarli, R., Gavazzi, G., Arosio, I., Cortese, L., Boselli, A., Bonfanti, C., & Colpi, M. 2007, *MNRAS*, 381, 136
- Dalla Vecchia, C., Bower, R. G., Theuns, T., Balogh, M. L., Mazzotta, P., & Frenk, C. S. 2004, *MNRAS*, 355, 995
- De Lucia, G., Springel, V., White, S. D. M., Croton, D., & Kauffmann, G. 2006, *MNRAS*, 366, 499
- Dickey, J. M. & Lockman, F. J. 1990, *ARA&A*, 28, 215
- Di Matteo, T., Allen, S. W., Fabian, A. C., Wilson, A. S., & Young, A. J. 2003, *ApJ*, 582, 133



- Di Matteo, T., Quataert, E., Allen, S. W., Narayan, R., & Fabian, A. C. 2000, *MNRAS*, 311, 507
- Dudik, R. P., Satyapal, S., Gliozzi, M., & Sambruna, R. M. 2005, *ApJ*, 620, 113
- Erwin, P. 2004, *A&A*, 415, 941
- Fabbiano, G. & Juda, J. Z. 1997, *ApJ*, 476, 666
- Ferrarese, L., Côté, P., Dalla Bontà, E., Peng, E. W., Merritt, D., Jordán, A., Blakeslee, J. P., Hasegan, M., Mei, S., Piatek, S., Tonry, J. L., & West, M. J. 2006, *ApJ*, 644, L21
- Ferrarese, L., Côté, P., Jordán, A., Peng, E. W., Blakeslee, J. P., Piatek, S., Mei, S., Merritt, D., Milosavljević, M., Tonry, J. L., & West, M. J. 2006, *ApJS*, 164, 334
- Ferrarese, L. & Ford, H. 2005, *Space Science Reviews*, 116, 523 (FF05)
- Ferrarese, L. & Merritt, D. 2000, *ApJ*, 539, L9
- Filippenko, A. V. & Ho, L. C. 2003, *ApJ*, 588, L13
- Finoguenov, A. & Jones, C. 2001, *ApJ*, 547, L107
- Fukugita, M., Ichikawa, T., Gunn, J. E., Doi, M., Shimasaku, K., & Schneider, D. P. 1996, *AJ*, 111, 1748
- Garmire, G., Feigelson, E. D., Broos, P., Hillenbrand, L. A., Pravdo, S. H., Townsley, L., & Tsuboi, Y. 2000, *AJ*, 120, 1426
- Gavazzi, G., Franzetti, P., Scodreggio, M., Boselli, A., Pierini, D., Baffa, C., Lisi, F., & Hunt, L. K. 1999, *VizieR Online Data Catalog*, 414, 20065 (Ga99)
- Gebhardt, K., Rich, R. M., & Ho, L. C. 2002, *ApJ*, 578, L41
- Gebhardt, K., Lauer, T. R., Kormendy, J., Pinkney, J., Bower, G. A., Green, R., Gull, T., Hutchings, J. B., Kaiser, M. E., Nelson, C. H., Richstone, D., & Weistrop, D. 2001, *AJ*, 122, 2469
- Gebhardt, K., Kormendy, J., Ho, L. C., Bender, R., Bower, G., Dressler, A., Faber, S. M., Filippenko, A. V., Green, R., Grillmair, C., Lauer, T. R., Magorrian, J., Pinkney, J., Richstone, D., & Tremaine, S. 2000, *ApJ*, 543, L5
- Geha, M., Guhathakurta, P., & van der Marel, R. P. 2002, *AJ*, 124, 3073
- Gehrels, N. 1986, *ApJ*, 303, 336
- Gerssen, J., van der Marel, R. P., Gebhardt, K., Guhathakurta, P., Peterson, R. C., & Pryor, C. 2002, *AJ*, 124, 3270
- Gilfanov, M. 2004, *MNRAS*, 349, 146
- Graham, A. W., Erwin, P., Caon, N., & Trujillo, I. 2001, *ApJ*, 563, L11
- Greene, J. E. & Ho, L. C. 2007a, *ApJ*, in press (arXiv0707.2617G)
- Greene, J. E. & Ho, L. C. 2007b, *ApJ*, 667, 131
- Häring, N. & Rix, H.-W., 2004, *ApJ*, 604, L89
- Heckman, T. M., Kauffmann, G., Brinchmann, J., Charlot, S., Tremonti, C., & White, S. D. M. 2004, *ApJ*, 613, 109
- Ho, L. C., Feigelson, E. D., Townsley, L. K., Sambruna, R. M., Garmire, G. P., Brandt, W. N., Filippenko, A. V., Griffiths, R. E., Ptak, A. F., & Sargent, W. L. W. 2001, *ApJ*, 549, L51
- Hong, J., van den Berg, M., Schlegel, E. M., Grindlay, J. E., Koenig, X., Laycock, S., & Zhao, P. 2005, *ApJ*, 635, 907
- Ichimaru, S. 1977, *ApJ*, 214, 840
- Juneau, S., Glazebrook, K., Crampton, D., McCarthy, P. J., Savaglio, S., Abraham, R., Carlberg, R. G., Chen, H.-W., Le Borgne, D., Marzke, R. O., Roth, K., Jørgensen, I., Hook, I., & Murowinski, R. 2005, *ApJ*, 619, L135
- Kollmeier, J. A., Onken, C. A., Kochanek, C. S., Gould, A., Weinberg, D. H., Dietrich, M., Cool, R., Dey, A., Eisenstein, D. J., Jannuzi, B. T., Le Floch, E., & Stern, D. 2006, *ApJ*, 648, 128
- Kormendy, J., Bender, R., Magorrian, J., Tremaine, S., Gebhardt, K., Richstone, D., Dressler, A., Faber, S. M., Grillmair, C., & Lauer, T. R. 1997, *ApJ*, 482, L139
- Kormendy, J. & Richstone, D. 1995, *ARA&A*, 33, 581
- Lauer, T. R., Faber, S. M., Richstone, D., Gebhardt, K., Tremaine, S., Postman, M., Dressler, A., Aller, M. C., Filippenko, A. V., Green, R., Ho, L. C., Kormendy, J., Magorrian, J., & Pinkney, J. 2007a, *ApJ*, 662, 808
- Lauer, T. R., Gebhardt, K., Faber, S. M., Richstone, D., Tremaine, S., Kormendy, J., Aller, M. C., Bender, R., Dressler, A., Filippenko, A. V., Green, R., & Ho, L. C. 2007b, *ApJ*, 664, 226
- Lauer, T. R., Tremaine, S., Ajhar, E. A., Bender, R., Dressler, A., Faber, S. M., Gebhardt, K., Grillmair, C. J., Kormendy, J., & Richstone, D. 1996, *ApJ*, 471, L79
- Loewenstein, M., Mushotzky, R. F., Angelini, L., Arnaud, K. A., & Quataert, E. 2001, *ApJ*, 555, L21
- Lodato, G. & Natarajan, P. 2006, *MNRAS*, 371, 1813
- Madau, P. & Rees, M. J. 2001, *ApJ*, 551, L27
- Maoz, D., Koratkar, A., Shields, J. C., Ho, L. C., Filippenko, A. V., & Sternberg, A. 1998, *AJ*, 116, 55
- McNamara, B. R. & Nulsen, P. E. J. 2007, *ARA&A*, 45, 117
- Marconi, A. & Hunt, L. K. 2003, *ApJ*, 589, L21
- Marconi, A., Risaliti, G., Gilli, R., Hunt, L. K., Maiolino, R., & Salvati, M. 2004, 222, 49
- MacArthur, L. A., Ellis, R. S., Treu, T., U, V., Bundy, K., Moran, S. M. 2007, *ApJ*, submitted
- McLure, R. J. & Dunlop, J. S. 2002, *MNRAS*, 331, 795
- Mei, S., Blakeslee, J. P., Côté, P., Tonry, J. L., West, M. J., Ferrarese, L., Jordán, A., Peng, E. W., Anthony, A., & Merritt, D. 2007, *ApJ*, 655, 144
- Merloni, A. & Heinz, S. 2007, *MNRAS*, 381, 589
- Miller, J. 2005, *AS&S*, 300, 227-238
- Narayan, R. & Yi, I. 1994, *ApJ*, 428, L13
- Pellegrini, S. 2005, *ApJ*, 624, 155
- Peng, C. Y., Ho, L. C., Impey, C. D., & Rix, H.-W. 2002, *AJ*, 124, 266
- Peterson, B. M. et al. , 2005, *ApJ*, 632, 799
- Randall, S. W., Sarazin, C. L., & Irwin, J. A. 2004, *ApJ*, 600, 729
- Rosati, P., Tozzi, P., Giacconi, R., Gilli, R., Hasinger, G., Kewley, L., Mainieri, V., Nonino, M., Norman, C., Szokoly, G., Wang, J. X., Zirm, A., Bergeron, J., Borgani, S., Gilmozzi, R., Grogin, N., Koekemoer, A., Schreier, E., & Zheng, W. 2002, *ApJ*, 566, 667
- Santra, S., Sanders, J. S., & Fabian, A. C. 2007, *MNRAS*, 382, 895
- Sijacki, D., Springel, V., di Matteo, T., & Hernquist, L. 2007, *MNRAS*, 380, 877
- Sivakoff, G. R., Jordán, A., Sarazin, C. L., Blakeslee, J. P., Côté, P., Ferrarese, L., Juett, A. M., Mei, S., & Peng, E. W. 2007, *ApJ*, 660, 1246
- Sivakoff, G. R., Sarazin, C. L., & Irwin, J. A. 2003, *ApJ*, 599, 218
- Soldatenkov, D. A., Vikhlinin, A. A., & Pavlinsky, M. N. 2003, *Astronomy Letters*, 29, 298
- Soltan, A. 1982, *MNRAS*, 200, 115
- Soria, R., Graham, A. W., Fabbiano, G., Baldi, A., Elvis, M., Jerjen, H., Pellegrini, S., & Siemiginowska, A. 2006a, *ApJ*, 640, 143
- Soria, R., Graham, A. W., Fabbiano, G., Baldi, A., Elvis, M., Jerjen, H., Pellegrini, S., & Siemiginowska, A. 2006b, *ApJ*, 640, 126
- Springel, V., White, S. D. M., & Hernquist, L. 2004, 220, 421
- Sulkkanen, M. E. & Bregman, J. N. 2001, *ApJ*, 548, L131
- Tremaine, S., Gebhardt, K., Bender, R., Bower, G., Dressler, A., Faber, S. M., Filippenko, A. V., Green, R., Grillmair, C., Ho, L. C., Kormendy, J., Lauer, T. R., Magorrian, J., Pinkney, J., & Richstone, D. 2002, *ApJ*, 574, 740
- Treu, T., Ellis, R. S., Liao, T. X., van Dokkum, P. G., Tozzi, P., Coil, A., Newman, J., Cooper, M. C., & Davis, M. 2005a, *ApJ*, 633, 174
- Treu, T., Ellis, R. S., Liao, T. X., van Dokkum, 2005b, *ApJ*, 622, 5
- Valluri, M., Ferrarese, L., Merritt, D., & Joseph, C. L. 2005, *ApJ*, 628, 137
- Volonteri, M., Haardt, F., & Gultekin, K. 2007, *MNRAS* submitted (arXiv0710.5770)
- Volonteri, M., Lodato, G., & Natarajan, P. 2007, *MNRAS* submitted (arXiv0709.0529)
- Xu, Y., Xu, H., Zhang, Z., Kundu, A., Wang, Y., & Wu, X.-P. 2005, *ApJ*, 631, 809
- Woo, J.-H. & Urry, C. M. 2002, *ApJ*, 579, 530
- Wilson, A. S. & Yang, Y. 2002, *ApJ*, 568, 133
- Zhao, P., Grindlay, J. E., Hong, J. S., Laycock, S., Koenig, X. P., Schlegel, E. M., & van den Berg, M. 2005, *ApJS*, 161, 429